EUROPEAN ORGANIZATION FOR NUCLEAR RESEARCH
CERN-PH-EP/2007-015
5 June 2007

Measurements of the Ξ^0 Lifetime and the $\overline{\Xi^0}/\Xi^0$ Flux Ratio in a Neutral Beam

NA48/1 Collaboration

J.R. Batley, G.E. Kalmus [1], C. Lazzeroni, D.J. Munday, M. Patel, M.W. Slater, S.A. Wotton

Cavendish Laboratory, University of Cambridge, Cambridge, CB3 0HE, U.K. [2]

R. Arcidiacono [3], G. Bocquet, A. Ceccucci, D. Cundy [4], N. Doble [5], V. Falaleev, L. Gatignon, A. Gonidec, P. Grafström, W. Kubischta, I. Mikulec [6], A. Norton, B. Panzer-Steindel, P. Rubin [7], H. Wahl [8]

CERN, CH-1211 Genève 23, Switzerland

E. Goudzovski [5], P. Hristov [9], V. Kekelidze, L. Litov, D. Madigozhin, N. Molokanova, Yu. Potrebenikov, S. Stoynev, A. Zinchenko

Joint Institute for Nuclear Research, Dubna, Russian Federation

E. Monnier [10], E. Swallow, R. Winston [11]

The Enrico Fermi Institute, The University of Chicago, Chicago, IL 60126, U.S.A.

R. Sacco [12], A. Walker

Department of Physics and Astronomy, University of Edinburgh, JCMB King's Buildings, Mayfield Road, Edinburgh, EH9 3JZ, U.K.

W. Baldini, P. Dalpiaz, P.L. Frabetti [13], A. Gianoli, M. Martini, F. Petrucci, M. Savrié, M. Scarpa

Dipartimento di Fisica dell'Università e Sezione dell'INFN di Ferrara, I-44100 Ferrara, Italy

A. Bizzeti [14], M. Calvetti, G. Collazuol [5], E. Iacopini, M. Lenti, G. Ruggiero [9], M. Veltri [15]

Dipartimento di Fisica dell'Università e Sezione dell'INFN di Firenze, I-50125 Firenze, Italy

M. Behler, K. Eppard, M. Eppard [9], A. Hirstius [9], K. Kleinknecht, U. Koch, P. Marouelli, L. Masetti [16], U. Moosbrugger, C. Morales Morales, A. Peters [9], R. Wanke *, A. Winhart

Institut für Physik, Universität Mainz, D-55099 Mainz, Germany [17]

A. Dabrowski, T. Fonseca Martin [9], M. Velasco

Department of Physics and Astronomy, Northwestern Uniwersity, Evanston, IL 60208-3112, U.S.A.

G. Anzivino, P. Cenci, E. Imbergamo, G. Lamanna [5], P. Lubrano, A. Michetti, A. Nappi, M. Pepe, M.C. Petrucci, M. Piccini [9], M. Valdata

Dipartimento di Fisica dell'Università e Sezione dell'INFN di Perugia, I-06100 Perugia, Italy

C. Cerri, F. Costantini, R. Fantechi, L. Fiorini [18], S. Giudici, I. Mannelli, G. Pierazzini, M. Sozzi

Dipartimento di Fisica, Scuola Normale Superiore e Sezione dell'INFN di Pisa, I-56100 Pisa, Italy

C. Cheshkov, J.B. Cheze, M. De Beer, P. Debu, G. Gouge, G. Marel, E. Mazzucato, B. Peyaud, B. Vallage

DSM/DAPNIA - CEA Saclay, F-91191 Gif-sur-Yvette, France

M. Holder, A. Maier [9], M. Ziolkowski

Fachbereich Physik, Universität Siegen, D-57068 Siegen, Germany [19]

C. Biino, N. Cartiglia, M. Clemencic [9], S. Goy Lopez [9], F. Marchetto, E. Menichetti, N. Pastrone

Dipartimento di Fisica Sperimentale dell'Università e Sezione dell'INFN di Torino, I-10125 Torino, Italy

W. Wislicki

Soltan Institute for Nuclear Studies, Laboratory for High Energy Physics, PL-00-681 Warsaw, Poland[20]

H. Dibon, M. Jeitler, M. Markytan, G. Neuhofer, L. Widhalm

Österreichische Akademie der Wissenschaften, Institut für Hochenergiephysik, A-1050 Wien, Austria[21]

Abstract

A total of 235698 $\Xi^0 \to \Lambda\pi^0$ and 21527 $\overline{\Xi^0} \to \overline{\Lambda}\pi^0$ decays were selected from data obtained by the NA48/1 experiment at CERN. From this sample, the lifetime of the Ξ^0 hyperon was measured to be $(3.065 \pm 0.012_{\rm stat} \pm 0.014_{\rm syst}) \times 10^{-10}$ s. This result is about two standard deviations above the world average and an order of magnitude more precise than the previous best measurement. With the same data sample, we have measured the ratio of $\overline{\Xi^0}$ and Ξ^0 fluxes in proton collisions at 400 GeV/c on a beryllium target.

1 Introduction

The lifetime of the doubly strangeness-carrying neutral hyperon Ξ^0 is an important input to measurements of other Ξ^0 parameters. As an example, when converting the branching fraction of Ξ^0 beta-decays into the corresponding partial decay width to extract the parameter $|V_{us}|$, the total Ξ^0 decay rate error represents one of the largest external uncertainties.

Several experiments in the 1960's and 70's measured the Ξ^0 lifetime, yielding a world average of $\tau_{\Xi^0} = (2.90 \pm 0.09) \times 10^{-10}$ s [1], based on an integrated data sample

* Corresponding author. *Email address:* Rainer.Wanke@uni-mainz.de
[1] Present address: Rutherford Appleton Laboratory, Chilton, Didcot, Oxon, OX11 0QX, U.K.
[2] Funded by the U.K. Particle Physics and Astronomy Research Council.
[3] Present address: Dipartimento di Fisica Sperimentale dell'Università e Sezione dell'INFN di Torino, I-10125 Torino, Italy
[4] Present address: Istituto di Cosmogeofisica del CNR di Torino, I-10133 Torino, Italy
[5] Present address: Dipartimento di Fisica, Scuola Normale Superiore e Sezione dell'INFN di Pisa, I-56100 Pisa, Italy
[6] On leave from Österreichische Akademie der Wissenschaften, Institut für Hochenergiephysik, A-1050 Wien, Austria
[7] On leave from University of Richmond, Richmond, VA, 23173, USA; supported in part by the US NSF under award #0140230. Present address: Department of Physics and Astronomy, George Mason University, Fairfax, VA 22030A, USA.
[8] Present address: Dipartimento di Fisica dell'Università e Sezione dell'INFN di Ferrara, I-44100 Ferrara, Italy
[9] Present address: CERN, CH-1211 Genève 23, Switzerland
[10] Present address: Centre de Physique des Particules de Marseille, IN2P3-CNRS, Université de la Méditerranée, Marseille, France.
[11] Also at University of California, Merced, U.S.A.
[12] Present address: Department of Physics, Queen Mary University, London, E1 4NS, U.K.
[13] Present address: Joint Institute for Nuclear Research, Dubna, 141980, Russian Federation
[14] Dipartimento di Fisica dell'Università di Modena e Reggio Emilia, I-41100 Modena, Italy
[15] Istituto di Fisica dell'Università di Urbino, I-61029 Urbino, Italy
[16] Present address: Physikalisches Institut, Universität Bonn, D-53115 Bonn, Germany
[17] Funded by the German Federal Minister for Research and Technology (BMBF) under contract 7MZ18P(4)-TP2
[18] Present address: Cavendish Laboratory, University of Cambridge, Cambridge, CB3 0HE, U.K.
[19] Funded by the German Federal Minister for Research and Technology (BMBF) under contract 056SI74
[20] Supported by the Committee for Scientific Research grants 5P03B10120, SPUB-M/CERN/P03/DZ210/2000 and SPB/CERN/P03/DZ146/2002
[21] Funded by the Austrian Ministry for Traffic and Research under the contract GZ 616.360/2-IV GZ 616.363/2-VIII, and by the Fonds für Wissenschaft und Forschung FWF Nr. P08929-PHY

of less than 8000 events. In the last 30 years, no new measurements of the Ξ^0 lifetime have been published.

Here we report on the precise measurement of the Ξ^0 and $\overline{\Xi^0}$ lifetimes, using data samples recorded with a minimum bias trigger by the NA48/1 experiment in the year 2002. From the same data set we have also determined the Ξ^0 and $\overline{\Xi^0}$ fluxes and their ratio as function of the energy.

2 Experimental Set-up

The NA48/1 experiment took data in 2002 at the CERN SPS. A beam of neutral particles was produced by a 400 GeV/c proton beam impinging on a Be target in 4.8 s long spills repeated every 16.8 s. The proton beam intensity had a mean of 5×10^{10} particles per pulse and was fairly constant over the duration of the spill.

In the NA48/1 set-up, only the K_S target station of the NA48 double K_S/K_L beam line was used [2]. A sweeping magnet deflected charged particles away from the collimators, which selected a beam of neutral long-lived particles (K_S, K_L, Λ, Ξ^0, n, and γ). The defining collimator was located 5.03 m down-stream of the target and had a circular aperture of 1.8 mm radius, followed by a final collimator, ending 6.23 m down-stream of the target with a radius of 3 mm. To reduce the number of photons, a 24 mm thick platinum absorber was placed between the target and the collimators. The target and collimator positions were chosen in such a way, that the beam axis passed through the centre of the electromagnetic calorimeter. The production angle between the proton beam direction and the axis of the neutral beam was 4.2 mrad. A right-handed coordinate system is defined with the z-axis pointing in direction of the former K_L beam and the y-axis pointing upwards.

The collimator was followed by a 90 m long evacuated tank, with a diameter between 1.92 and 2.4 m and terminated by a 0.3% X_0 thick Kevlar window. The detectors were located down-stream of this region to detect the products of the particles decaying in the volume contained by the tank. On average, about 1.4×10^4 Ξ^0 hyperons per spill decayed in the fiducial decay volume, dominantly into the $\Lambda\pi^0$ final state used in this analysis.

The momenta and positions of charged particles were measured in a magnetic spectrometer. The spectrometer was housed in a helium gas volume and consisted of two drift chambers before and two after a dipole magnet with vertical magnetic field direction, giving a horizontal transverse momentum kick of 265 MeV/c. Each chamber had four views (x, y, u, v) with two sense wire planes each. The u and v views are inclined by $\pm 45^\circ$ with respect to the x-y plane. In the chamber located just down-stream of the magnet, only x and y views were instrumented. The space points, reconstructed by each chamber, had a resolution of 150 μm in each projection. The momentum resolution of the spectrometer was measured to be $\sigma_p/p = 0.48\% \oplus 0.015\% \times p$, with p in GeV/c. The track time resolution was about 1.5 ns.

Photons were measured with a 27 radiation lengths deep liquid-krypton electromagnetic calorimeter (LKr). It was read out longitudinally in about 13500 cells of cross-section 2×2 cm^2. The energy resolution was determined to be $\sigma_E/E =$

$3.2\%/\sqrt{E} \oplus 9\%/E \oplus 0.42\%$, with E in GeV. The spatial and time resolutions were better than 1.3 mm and 300 ps, respectively, for photons with energies above 20 GeV.

Other detector elements were only used at the trigger level. An iron-scintillator sandwich hadron calorimeter, 6.7 nuclear interaction lengths thick, followed downstream of the LKr. It provided a raw measurement of the energy of hadron showers. A segmented scintillator hodoscope for charged particles, with a time resolution better than 200 ps for two-track events, was located between the spectrometer and the LKr calorimeter. Also, seven rings of scintillation counters (AKL) were placed around the decay volume and the helium tank of the spectrometer to detect activity outside of the detector acceptance. A more detailed description of the NA48/1 beam-line and detector can be found in [2].

The events used in the analysis described here were selected with a minimum bias trigger. This trigger required at least one hit in the hodoscope for charged particles, a hit pattern in the drift chambers consistent with coming from two charged tracks, no hit in either of the last two rings of the AKL, and energy depositions of either 15 GeV in the LKr calorimeter or 30 GeV in the LKr and hadron calorimeter together. This minimum bias trigger was down-scaled by a factor of 35. The trigger efficiency for the $\Xi^0 \to \Lambda\pi^0$ selection was determined to be $(99.77 \pm 0.03)\%$, with no observed dependency on the spectrometer polarity.

In addition, a software trigger was applied for $\Xi^0 \to \Lambda\pi^0$ candidates. This trigger performed a rough selection using on-line track and cluster information. The efficiency of the software trigger was measured to be $(99.88 \pm 0.05)\%$.

After applying the trigger selection, the data sample consisted of about 1.2×10^7 minimum bias events with exactly 2 tracks, 1 vertex, and 2 or more unassociated clusters.

3 Data Selection

The $\Xi^0 \to \Lambda\pi^0$ candidates were reconstructed via the decays $\Lambda \to p\pi^-$ and $\pi^0 \to \gamma\gamma$. Each selected event had to have exactly 2 oppositely charged tracks and exactly 2 unassociated clusters in the LKr calorimeter.

The positive track (proton) had to have a momentum $p_p > 30$ GeV/c, the negative track (pion) was required to have $p_{\pi^-} > 4$ GeV/c. The momentum ratio p_+/p_- between positive and negative tracks had to exceed 4.

Both tracks were required to have a radial distance from the detector axis between 13 and 120 cm in each drift chamber. The distance between the tracks had to be greater than 5 cm in the first drift chamber and different from zero in the last chamber to reject so-called ghost tracks, which share track segments. To reject electrons, the tracks had to have either no associated cluster in the LKr calorimeter or a ratio of cluster energy over momentum less than 0.8. The distance of closest approach between the tracks had to be less than 2.2 cm, and the time difference Δt_{tracks} between the tracks had to be less than 2 ns. Finally, the invariant mass of the two tracks under proton and π^- assumption had to be between 1.112 and 1.120 GeV/c^2, corresponding to a 4σ window around the nominal Λ mass.

Each photon cluster was required to have a reconstructed energy between 3 and 120 GeV and to lie well inside the active LKr calorimeter region in a distance between 15 and 110 cm from the detector axis. The closest distance to any dead cell had to be larger than 2 cm. Each photon cluster had to have a distance greater than 40 cm to any track impact point at the face of the LKr. The distance between the two clusters had to be larger than 10 cm and their time difference had to be less than 4 ns. The difference between the mean track and mean cluster time had to be less than 3 ns.

An energy centre-of-gravity

$$(x_{\rm cog}, y_{\rm cog}) \;=\; \left(\frac{\sum_i x_i E_i}{\sum_i E_i}, \frac{\sum_i y_i E_i}{\sum_i E_i} \right)$$

at the longitudinal position of the LKr is defined by using the transverse positions x_i and y_i and the energies E_i of the photon clusters and tracks at the front surface of the LKr calorimeter. The tracks are projected onto the LKr surface from their positions and momenta in the first drift chamber before the spectrometer magnet. To suppress badly measured events and possible background, the radial distance $r_{\rm cog} = \sqrt{x_{\rm cog}^2 + y_{\rm cog}^2}$ of the energy centre-of-gravity to the beam axis was required to be less than 5 cm.

The Λ direction-of-flight is reconstructed from the momenta and track positions in the first drift chamber, while the Ξ^0 line-of-flight is determined by the line connecting the target with the energy centre-of-gravity $(x_{\rm cog}, y_{\rm cog})$ in the LKr calorimeter. The Ξ^0 decay vertex is then defined to be at the position of the closest distance of approach of the Λ and the Ξ^0 flight paths. Using the Ξ^0 vertex reconstructed in this way, a cut on the $\gamma\gamma$ invariant mass of $125 < m_{\gamma\gamma} < 145$ MeV/c^2 was applied, corresponding to a 3σ window around the nominal π^0 mass. Finally, a loose cut on the $\Lambda\pi^0$ invariant mass was applied: $1.305 < m_{\Lambda\pi^0} < 1.325$ GeV/c^2.

Applying all selection criteria yielded a final data sample of 235698 events, which was practically background-free, and on which the lifetime measurement was performed (Fig. 1).

4 Monte Carlo Simulation

A Monte Carlo simulation was performed with the full detector description, using GEANT3 [3], but without trigger simulation. In total, 10^9 $\Xi^0 \to \Lambda\pi^0$ events were generated, from which 4.0×10^6 were reconstructed after the complete selection, corresponding to about 17 times the data sample. The mean Ξ^0 lifetime used in the simulation was $\tau_{\Xi^0}^{\rm MC} = 3.19 \times 10^{-10}$ s. This was chosen to be 10% higher than the current world average of previous measurements [1] in order to ensure sufficient Monte Carlo statistics also at high lifetime values.

The production plane is the y-z plane; symmetry arguments imply that there is no Ξ^0 polarisation in y or z. For the Ξ^0 polarisation in x direction, a value of $P_x = -10\%$ was used. This is in agreement with the measured value of $P_x^{\Xi^0} = (-9.7 \pm 0.7 \pm 1.3)\%$ for an unpolarised proton beam with energy of 800 GeV and a production angle

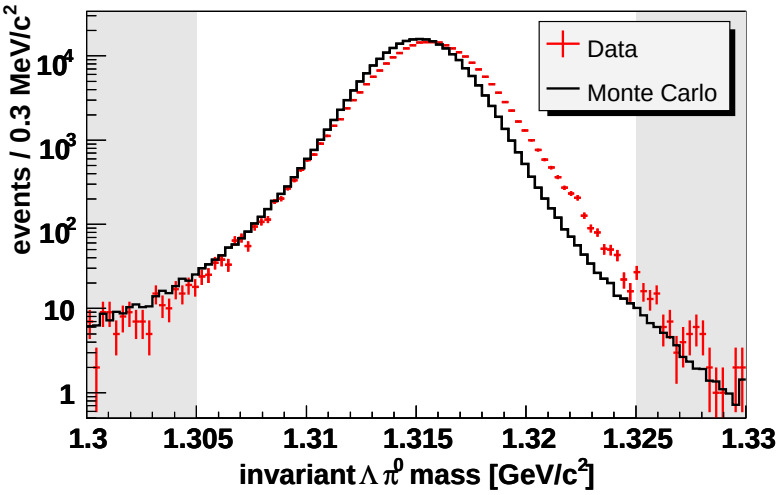

Fig. 1. Invariant $\Lambda\pi^0$ mass of the selected Ξ^0 candidates for data and simulation. The shaded areas are rejected by the mass cut. For the mean Ξ^0 mass of the simulated events see Section 4.

of 4.8 mrad [5]. For $\overline{\Xi^0}$ hyperons, no polarisation in the x direction was assumed in agreement with the same KTeV measurement. For the decay asymmetry of the $\Xi^0 \to \Lambda\pi^0$ and the subsequent $\Lambda \to p\pi^-$ decay the world averages of $\alpha(\Xi^0 \to \Lambda\pi^0) = -0.411 \pm 0.022$ and $\alpha_-(\Lambda \to p\pi^-) = -0.642 \pm 0.013$ were used [1].

The Ξ^0 beam profile is not perfectly simulated; it depends critically on precise knowledge of the geometry of the target and collimator region and the beam. Therefore, the simulated beam profile is somewhat narrower than that found in the data. This difference was taken into account by reweighting the simulated events with $r_{\rm cog} > 3.5$ cm. The applied weighting factors do not exceed 1.5.

The Ξ^0 mass spectrum of the data is shifted up by about 0.5 MeV/c^2 with respect to the simulation (Fig. 1). This corresponds to about 2.5 standard deviations from the previously measured value [4], which has been used in the simulation. We see this shift also in other Ξ^0 decay channels, but not for other decaying particles, e.g. neutral kaons. This effect is taken into account in the systematic uncertainty of the lifetime measurement.

Fig. 2 shows the Ξ^0 momentum spectra for reconstructed data and Monte Carlo events. Since the analysis is performed in energy bins, the small residual discrepancies in the momentum spectrum are of no importance.

5 Mean Lifetime Measurements

5.1 Measurement of the Ξ^0 Lifetime

In the experiment, the proper lifetime t of a particle with mass m, momentum p, and the decay length z is given by $t = z/\gamma\beta c = z\,m/p$, so for the lifetime both the momentum p and the decay vertex z have to be measured.

The most precise determination of the Ξ^0 decay vertex z comes from LKr calorime-

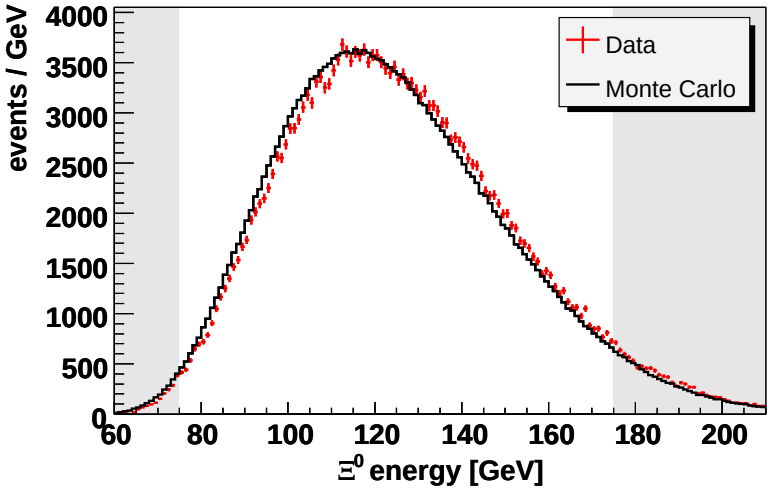

Fig. 2. Energy spectra of data and simulation for reconstructed $\Xi^0 \to \Lambda\pi^0$ events The shaded areas are not used in the lifetime fit.

ter information. By using the nominal π^0 mass, the decay vertex is obtained from

$$z = z_{\mathrm{LKr}} - \frac{1}{m_{\pi^0}} \sqrt{E_1 E_2 (\vec{r_1} - \vec{r_2})^2}, \tag{1}$$

with the longitudinal position z_{LKr} of the front edge of the LKr calorimeter and the energies E_1, E_2 and positions $\vec{r}_1, \vec{r}_2$ of the photon clusters. The vertex resolution is about 130 cm, as determined from simulation. The correct vertex resolution was verified by using the reconstructed edge of the final collimator: At this position the vertex distribution exhibits a step function (when neglecting the small number of reconstructed events, which decay inside the collimator), smeared by the resolution of the reconstructed decay vertex. The decay vertex distribution at the edge of the final collimator agrees well between real data and simulated data.

The distribution of proper lifetime of the selected Ξ^0 events is shown in Fig. 3. The lifetime is measured in units of the current world average of $\tau_{\Xi^0}^{\mathrm{PDG}} = 2.90 \times 10^{-10}$ s.

For the lifetime fit, the lifetime distribution of the data was compared to that of the Monte Carlo simulation. To be independent of the correct simulation of the Ξ^0 spectrum, the comparison was performed separately in ten 10 GeV wide bins of energy in the range from 75 to 175 GeV. For each energy bin, a fit region in proper lifetime was defined to allow for different detector acceptances and resolutions at different energies. The lower bound of each fit region was given by $t_{min} = 5$ m$/c + 0.7 \cdot \tau_{\Xi^0}^{\mathrm{PDG}}$ to ensure enough distance from the final collimator, where effects of scattering at the collimator edges and of different vertex resolutions between data and simulation play a role. The upper bound of each fit region was defined as $t_{max} = (9.4 - E/25\,\mathrm{GeV}) \cdot \tau_{\Xi^0}^{\mathrm{PDG}}$, but at most $5 \cdot \tau_{\Xi^0}^{\mathrm{PDG}}$. By these restrictions, in each bin of the proper time distributions there were at least 80 data and 2000 simulated events, respectively. A total of 126623 events were finally used for the lifetime fit. The distribution of the selected events in energy and proper time is shown in Fig. 4.

A combined least-squares fit to all lifetime distributions was performed, leaving

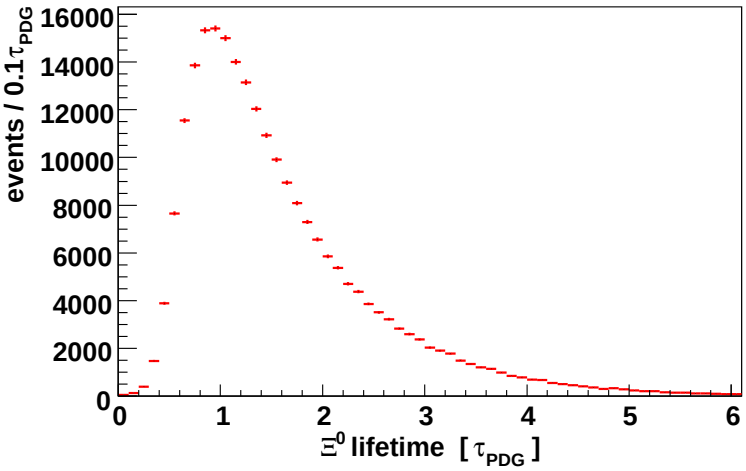

Fig. 3. Distribution of proper time of the selected Ξ^0 candidates in units of $\tau_{\rm PDG} = 2.9 \times 10^{-10}$ s.

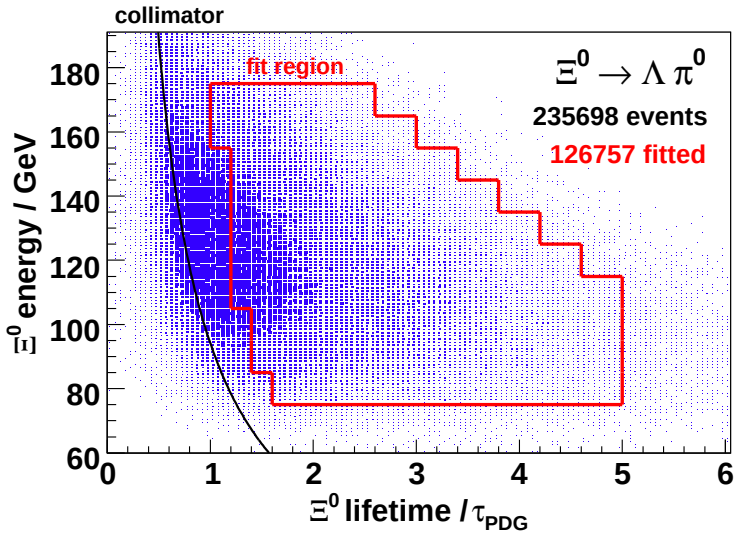

Fig. 4. Energy versus lifetime of accepted Ξ^0 events, measured from the target in units of $\tau_{\rm PDG} = 2.9 \times 10^{-10}$ s. The contour encloses the accepted region for the lifetime fit.

the mean Ξ^0 lifetime τ_{Ξ^0} and the 10 normalisations N_i of each energy bin as free parameters. The fit weighted reconstructed Monte Carlo events according to their proper time t with a factor $N_i \times \exp(-t/\tau_{\Xi^0})/\exp(-t/\tau_{\Xi^0}^{\rm MC})$ and compared the resulting distribution to the lifetime distribution found in data. The result of the fit is

$$\tau_{\Xi^0} \;=\; (1.0581 \pm 0.0044_{\rm stat}) \times \tau_{\Xi^0}^{\rm PDG} \;=\; (3.068 \pm 0.013_{\rm stat}) \times 10^{-10}\ {\rm s}, \qquad (2)$$

with the quoted error being only statistical. The fit has a $\chi^2/n_{\rm dof} = 135.9/135$. The residuals in each bin of energy are shown in Fig. 5.

We have also performed ten separate fits in the energy bins. These separate measurements agree with a $\chi^2/n_{\rm dof} = 12.4/9$, show no dependency on the Ξ^0 energy, and yield practically the same result as the global fit, when combined (see Fig 6).

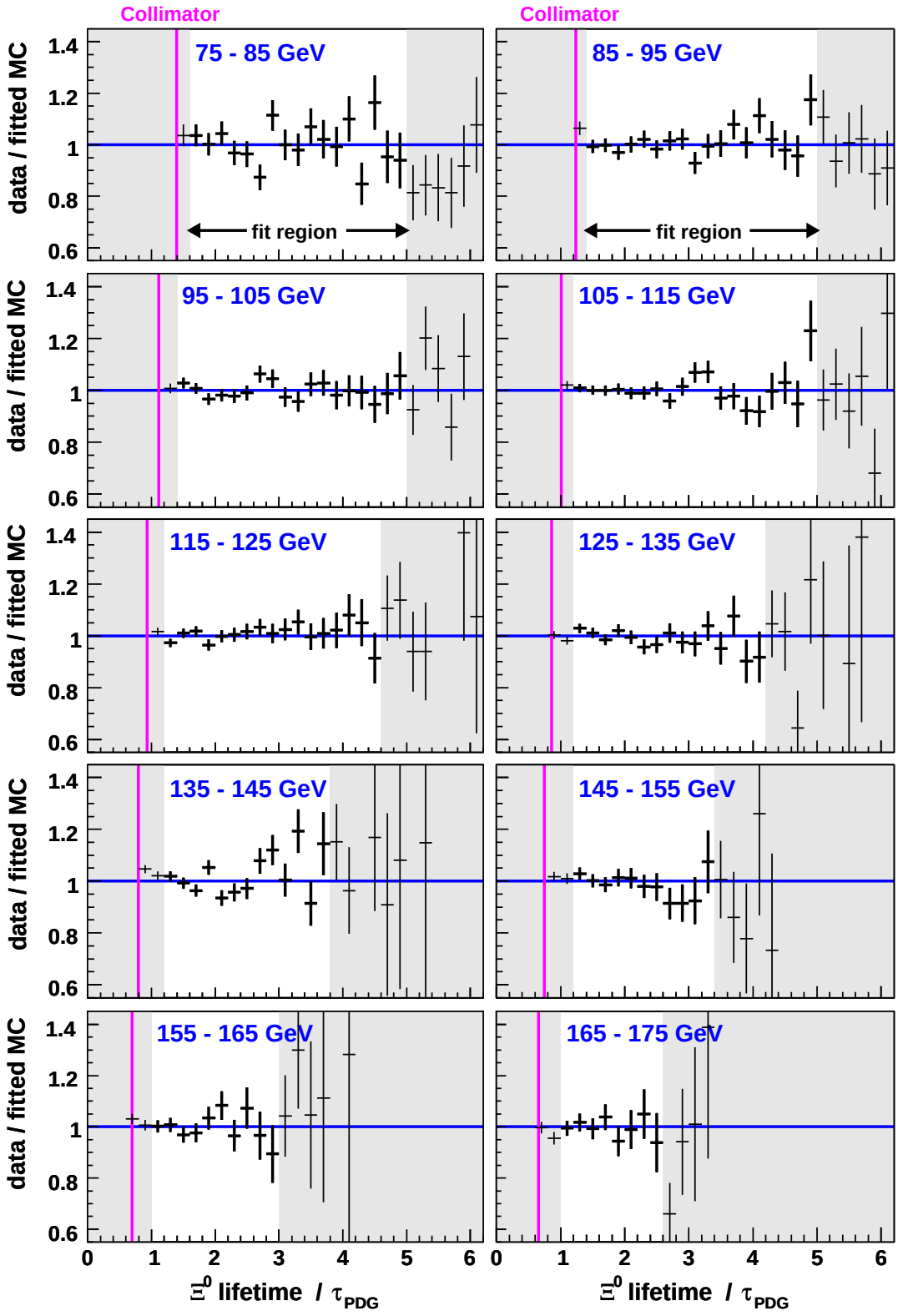

Fig. 5. Data lifetime distributions in units of $\tau_{\rm PDG} = 2.9 \times 10^{-10}$ s divided by the fitted distributions obtained by the Monte Carlo simulation. Indicated are the collimator position and the lifetime regions used for the fit.

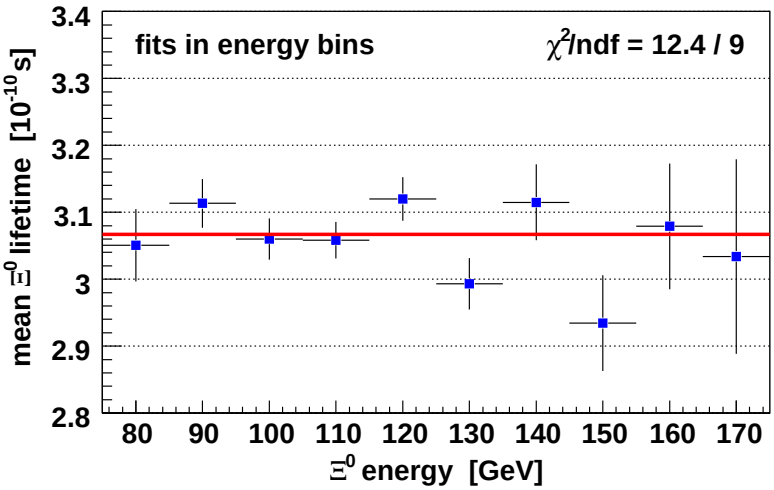

Fig. 6. Fit results for each bin of energy. The line indicates the combination of the separate results.

5.2 Systematic Uncertainties

Potential sources of systematic errors have been studied and several checks have been performed.

Possible imperfections of the description of the detector acceptance in the Monte Carlo simulation might cause systematic effects on the lifetime measurement. In particular, the criterion on the minimum radial track position in the drift chamber is sensitive to such possible MC imperfections, as it cuts directly into the acceptance. Varying this and other selection cuts, we found maximum changes of the result of the order of $\pm 0.3\%$, which we assign as systematic uncertainty due to the detector acceptance.

In the analysis, the energy scale of the LKr calorimeter was assumed to be exactly 1. Since the Ξ^0 decay vertex is determined using the π^0 decay into two photons, a wrong energy scale would directly affect the vertex determination and the lifetime measurement. The LKr energy scale is known to $\pm 0.1\%$ for the 2002 data, from which we determined an uncertainty of $\pm 0.14\%$ on the lifetime measurement.

Similarly, non-linearities in the shower energy reconstruction for low energy photons could affect the lifetime measurement. Using bounds for possible non-linearities derived from $K \to 2\pi^0/3\pi^0$, K_{e3}, and $\pi^0/\eta \to \gamma\gamma$ decays from data, we estimated an uncertainty of $\pm 0.09\%$ on the lifetime measurement. As a cross-check, the effect of varying the minimum photon energy was studied, and no variation of the result was seen.

The lifetime measurement is sensitive to the correct simulation of the vertex resolution. We checked the effect of a possible incorrect neutral vertex resolution by artificially increasing it by 5%, which is twice as much as is seen in the data when fitting the collimator edge. The effect on the result is a change of 0.08%. This number is used as an estimate for the systematic uncertainty due to the vertex resolution.

To estimate the systematic uncertainty from inaccurate knowledge of the Ξ^0 polar-

Effect	$\Delta_{\rm syst}\tau_{\Xi^0}$ [%]	$\Delta_{\rm syst}\tau_{\Xi^0}$ [10^{-10} s]
Detector acceptance	$\pm\,0.30$	$\pm\,0.009$
Vertex resolution	$\pm\,0.08$	$\pm\,0.002$
Energy scale	$\pm\,0.14$	$\pm\,0.004$
Energy non-linearities	$\pm\,0.09$	$\pm\,0.003$
Ξ^0 polarisation	$\pm\,0.24$	$\pm\,0.007$
Ξ^0 mass	$\pm\,0.20$	$\pm\,0.006$
Λ lifetime	$\pm\,0.04$	$\pm\,0.001$
Total systematic uncertainty	$\pm\,0.47$	$\pm\,0.014$
Statistical uncertainty	$\pm\,0.44$	$\pm\,0.013$

Table 1. Summary of systematic uncertainties.

isation, we refitted the lifetime distributions using Monte Carlo samples with 0 and -20% polarisation, respectively. The average of the observed deviations is $\pm 0.24\%$ and is taken as systematic uncertainty due to the Ξ^0 polarisation.

As pointed out earlier, we do see a shift in the invariant Ξ^0 mass w.r.t. the previously measured value. We generated Monte Carlo samples with $\pm 1\sigma$ around this value and also with the Ξ^0 mass seen in our data. Using these samples for the fit, the result changes by $\pm 0.20\%$, which we apply as systematic uncertainty.

Finally, the uncertainty on the measured Λ lifetime [1] affects the measurement by $\pm 0.04\%$ due to changes in the detector acceptance.

As additional cross-checks, the data were split into samples with different polarity of the spectrometer magnet and different run periods. No other than statistical variations were seen.

The summary of systematic uncertainties is given in Table 1. Adding all contributions in quadrature yields a total systematic uncertainty of $\Delta_{\rm syst} = \pm\,0.47\%$, corresponding to $\pm\,0.014 \times 10^{-10}$ s.

5.3 Measurement of the $\overline{\Xi^0}$ Lifetime

The mean lifetime of the $\overline{\Xi^0}$ hyperon was also measured through its decay to $\overline{\Lambda}\pi^0$. The $\overline{\Xi^0} \to \overline{\Lambda}\pi^0$ decays were selected using the same selection criteria as for the $\Xi^0 \to \Lambda\pi^0$ channel, but taking into account the reversed charges of the $\overline{\Lambda} \to \bar{p}\pi^+$ tracks. Applying all selection criteria yielded a final data sample of 21527 $\overline{\Xi^0} \to \overline{\Lambda}\pi^0$ decays (Fig. 7). The lifetime fit was performed completely analogous to the fit of the Ξ^0 lifetime, with 12246 events in the fitted region. However, since the number of $\overline{\Xi^0}$ is about a factor of 10 less than the number of Ξ^0, and the $\overline{\Xi^0}$ spectrum is peaked at lower energy than the Ξ^0 spectrum, many bins of the fit region have very few data events. Therefore, instead of a least-squares fit, a maximum-likelihood fit was performed, taking into account the poisson distribution of the data events.

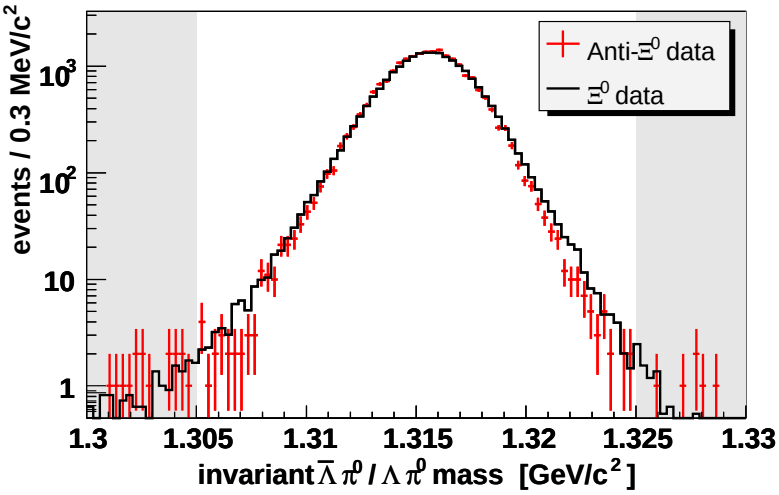

Fig. 7. Invariant $\overline{\Lambda}\pi^0$ mass of the selected data $\overline{\Xi^0}$ candidates. Also shown is the scaled distribution of selected $\Xi^0 \to \Lambda\pi^0$ events. The shaded areas are rejected by the selection criteria.

Performing the fit yielded

$$\tau_{\overline{\Xi^0}} \;=\; (1.0485 \pm 0.0130_{\text{stat}}) \times \tau_{\overline{\Xi^0}}^{\text{PDG}} \;=\; (3.041 \pm 0.038_{\text{stat}}) \times 10^{-10}\ \text{s}, \qquad (3)$$

in good agreement with the value measured for the Ξ^0 lifetime.

Since the systematic uncertainties have the same origin as those of the Ξ^0 lifetime measurement, they were assumed to be the same, and no separate estimation of the systematic uncertainty on the $\overline{\Xi^0}$ lifetime measurement has been performed, With this, the total systematic uncertainty on the $\overline{\Xi^0}$ lifetime is $\sigma_{\text{syst}} = \pm 0.014 \times 10^{-10}$ s.

6 Result and Implications of the Ξ^0 Lifetime Measurement

We have measured the mean lifetimes of the Ξ^0 hyperon $\tau_{\Xi^0} \;=\; (3.068 \pm 0.013_{\text{stat}} \pm 0.014_{\text{syst}}) \times 10^{-10}$ s and its anti-particle $\tau_{\overline{\Xi^0}} \;=\; (3.041 \pm 0.038_{\text{stat}} \pm 0.014_{\text{syst}}) \times 10^{-10}$ s. Under the assumption of CPT invariance both results can be combined, yielding

$$\tau_{\Xi^0} \;=\; (3.065 \pm 0.012_{\text{stat}} \pm 0.014_{\text{syst}}) \times 10^{-10}\ \text{s}, \qquad (4)$$

where all systematics except the Ξ^0 polarisation were taken as completely correlated.

This new result compared with the previous measurements is shown in Fig. 8. It lies almost two standard deviations above the previous world average and is an order of magnitude more precise than the previous best measurement. Compared to the previous world average, the precision is better by a factor of five.

Our new result does have implications on the measurements of $|V_{us}|$ from the β-decay $\Xi^0 \to \Sigma^+ e^- \bar{\nu}_e$. Taking the recent precise NA48/1 measurement on the $\Xi^0 \to \Sigma^+ e^- \bar{\nu}_e$ branching fraction of $(2.51 \pm 0.09) \times 10^{-4}$ [6], we obtain for the decay

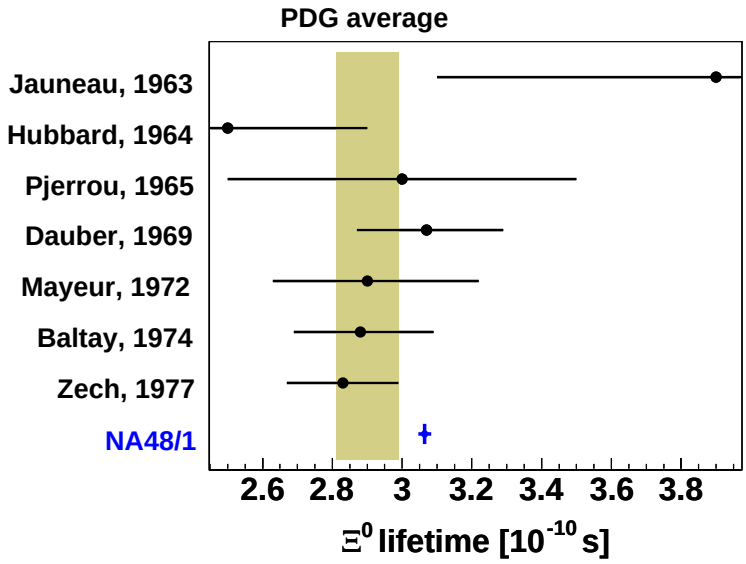

Fig. 8. Measurements of the Ξ^0 lifetime. For the previous measurements see [1].

rate

$$\Gamma(\Xi^0 \to \Sigma^+ e^- \bar{\nu}_e) \;=\; \frac{BR_{\Xi^0 \to \Sigma e \bar{\nu}}}{\tau_{\Xi^0}} \;=\; (8.19 \pm 0.30) \times 10^5\,\mathrm{s}^{-1}. \tag{5}$$

Performing the same calculation and using the same other inputs as in ref. [6], a value of

$$|V_{us}| \;=\; 0.203 \;\pm\; 0.004_{\mathrm{exp}}\;{}^{+0.022}_{-0.027\,\mathrm{form\ factors}} \tag{6}$$

is found, where the first error comes from our experimental measurements, and the second error from the uncertainty on the g_1 and f_1 form factors [7].

7 Measurement of the $\overline{\Xi^0}/\Xi^0$ Flux Ratio

The same data sample of $\Lambda\pi^0$ and $\overline{\Lambda}\pi^0$ decays used for the Ξ^0 lifetime measurement was also exploited to determine the production ratio between $\overline{\Xi^0}$ and Ξ^0 hyperons at the target. We applied the same selection criteria as for the lifetime measurement, except the requirements on the total energy and proper lifetime.

Fig. 9 shows the $\overline{\Xi^0}$ to Ξ^0 flux ratio as a function of energy. It falls with energy, as expected. The values in each energy bin are listed in Tab. 2.

8 Acknowledgements

It is a pleasure to thank the technical staff of the participating laboratories, universities, and affiliated computing centres for their efforts in the construction of the NA48 apparatus, in the operation of the experiment, and in the processing of the data.

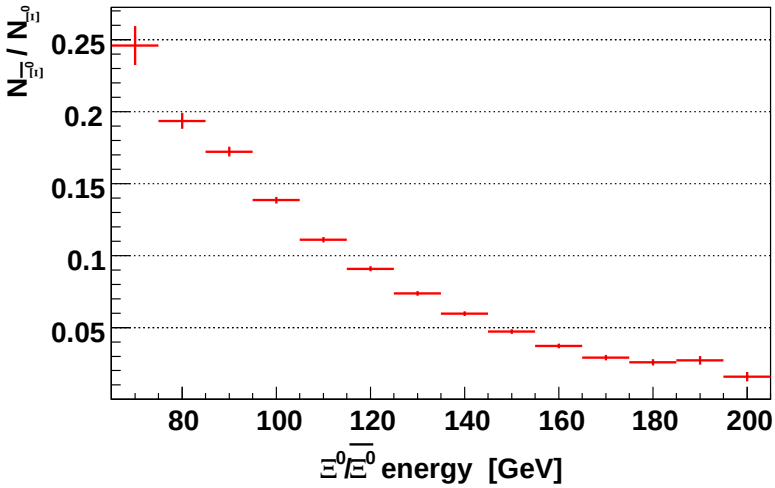

Fig. 9. Measurement of the $\overline{\Xi^0}$ to Ξ^0 flux ratio as function of energy.

Energy interval	$\overline{\Xi^0}/\Xi^0$ flux ratio
65 – 75 GeV	0.246 ± 0.014
75 – 85 GeV	0.194 ± 0.006
85 – 95 GeV	0.172 ± 0.003
95 – 105 GeV	0.139 ± 0.002
105 – 115 GeV	0.111 ± 0.002
115 – 125 GeV	0.091 ± 0.002
125 – 135 GeV	0.074 ± 0.002

Energy interval	$\overline{\Xi^0}/\Xi^0$ flux ratio
135 – 145 GeV	0.060 ± 0.002
145 – 155 GeV	0.047 ± 0.002
155 – 165 GeV	0.037 ± 0.002
165 – 175 GeV	0.029 ± 0.002
175 – 185 GeV	0.026 ± 0.002
185 – 195 GeV	0.027 ± 0.003
195 – 205 GeV	0.016 ± 0.003

Table 2. Tabulated values of the $\overline{\Xi^0}$ to Ξ^0 flux ratio as function of energy.

References

[1] W.M. Yao *et al.* (Particle Data Group), J. Phys. **G 33** (2006), 1.

[2] V. Fanti *et al.* (NA48 Collaboration), *Nucl. Instrum. Methods* A **574** (2007), 433.

[3] GEANT Detector Description and Simulation Tool, CERN Program Library Long Write-up W5013 (1994).

[4] V. Fanti *et al.* (NA48 Collaboration), *Eur. Phys. J.* C **C12** (2000), 69.

[5] T. Alexopoulos and A.R. Erwin, in: Proc. of the Hyperon Physics Symposion (Hyperon99), Batavia, IL, September 1999.

[6] J.R. Batley *et al.* (NA48/1 Collaboration), CERN-PH-EP/2006-032, accepted for publication by *Phys. Lett.* B.

[7] A. Alavi-Harati *et al.* (KTeV Collaboration), *Phys. Rev. Lett.* **87** (2001), 132001.